Applied Clay Science 271 (2025) 107811

Contents lists available at ScienceDirect

Applied Clay Science

journal homepage: www.elsevier.com/locate/clay

Research Paper

Synergistic effect of high-energy milling and organic intercalation on the kaolin properties and structural evolution

Alexandre Zaccaron [a,*], Fabiano Raupp-Pereira [a], Vitor de Souza Nandi [a], João C.C. Abrantes [b], Manuel J. Ribeiro [b], Adriano Michael Bernardin [a]

[a] Post-Graduate Program on Materials Science and Engineering (PPGCEM), Universidade do Extremo Sul Catarinense - UNESC, Avenida Universitária 1105, 88806-000 Criciúma, SC, Brazil

[b] proMetheus-Research Unit in Materials, Energy and Environment for Sustainability, Polytechnic Institute of Viana do Castelo, 4900-347 Viana do Castelo, Portugal

ARTICLE INFO

Keywords:
Kaolin
High-energy milling
Structure
Functionalization
Intercalation

ABSTRACT

Clays are raw materials with a wide range of applications in modern times. They can be used in various industrial applications, from the simplest to the most technological, such as in the ceramic industry to functionalizing components for the intercalation of organic molecules into polymeric matrices. Kaolinitic clays with a 1:1-layer structure is among the most abundant in the Earth's crust and are relatively easy to extract. Therefore, studies aimed at expanding the range of applications through the modification of the microstructure of these clay minerals have increasingly attracted scientific attention. The microstructural alteration of kaolinite through high-energy mechanical action can be an interesting method for mineral functionalization, as it leads to an increase in specific surface area and, consequently, the reactivity of the inorganic solid component. For this reason, this study investigated the effectiveness of the mechanical transformation process using high-purity kaolin, characterized before and after the high-energy milling process using XRF, XRD, DTA/TG, PSD, FTIR, and SEM techniques. The results showed that the milling process significantly altered the kaolinitic microstructure, demonstrating a reduction in particle size under the established experimental conditions, reaching $D_{90} \leq 1$ μm. By obtaining a reactive solid with a significantly increased specific surface area (18× increase through milling), a 2^k factorial experimental design was applied to study some variables of the intercalation process, such as the type of molecule (diaminomethanal - urea and dimethyl sulfoxide - DMSO), stirring time (from 12 to 24 h), and kaolinite mass (varying from 10 to 50 g) in a 100 mL solution. The microstructural characterization results via XRD revealed that the use of DMSO resulted in better efficacy in increasing basal spacing (from 7.2 Å to 11.3 Å with DMSO) and consequently in a possible application with functional groups.

1. Introduction

Clay is the oldest raw material used by humans, defined as a soil that transforms into a plastic paste when mixed with water. This paste is easily moldable, and once dried, it becomes hard and brittle, retaining its shape. Furthermore, when fired, it becomes even more resistant and impervious to water. Such material is clearly suitable for making items of all shapes (Worral, 1975).

Thus, these minerals are used as inputs in various economic activities and have a range of applications. In agriculture, they are primarily responsible for the fertilizers fixation and serve as a physical-mechanical support for plants. In livestock farming, they are included in animal feed. In industry, the application is more diverse and expressive, spanning all industrial classifications, from extractive to manufacturing, providing inputs for construction and even serving as raw material for chemical processing. The mineral wealth, combined with its great natural availability and other important properties (Santos de Santos, 1989), broadens its applications, depending on the chemical and mineralogical composition and the physicochemical characteristics, such as in cosmetology (da Silva Favero et al., 2019) and as nanocomposites in polymer matrices. In the latter form of application, they can significantly improve the properties of engineering materials made

* Corresponding author at: Post-Graduate Program on Materials Science and Engineering - PPGCEM, Universidade do Extremo Sul Catarinense, Criciúma, SC, Brazil.

E-mail addresses: alexandrezaccaron@hotmail.com (A. Zaccaron), jabrantes@estg.ipvc.pt (J.C.C. Abrantes), ribeiro@estg.ipvc.pt (M.J. Ribeiro), amb@unesc.net (A.M. Bernardin).

https://doi.org/10.1016/j.clay.2025.107811
Received 6 January 2025; Received in revised form 10 March 2025; Accepted 28 March 2025
Available online 1 April 2025

from polymers with low filler content. This technology has been widely applied commercially and has attracted great attention since the early 2000s (Gao, 2004). Consequently, the use of clay as a filler and reinforcement material for the production of polymer compounds has been extensively studied (Khan et al., 2020; Sanusi et al., 2020; Zare and Rhee, 2020).

The functionalization of clays is a method aimed at expanding the applications of these minerals. The organophilization process is the key step for achieving good dispersion and exfoliation of the clay mineral layers, which can increase hydrophobicity and the spacing between the clay layers (Zaharia et al., 2015). The organophilic nature reduces the specific surface energy and makes the clay more compatible with nonpolar organic polymers. Additionally, the increased basal spacing facilitates the intercalation of polymer chains between the clay layers (de Oliveira et al., 2018).

Studies on the interaction between clay minerals and organic compounds have been conducted since the early 20th century, further increasing the versatility of these materials. Bentonite is the most commonly used clay in the preparation of organophilic clays. This is due to the predominant presence of the clay mineral montmorillonite, which exhibits more favorable characteristics for interlamellar intercalation (de Paiva et al., 2008). Due to their high reactivity, they are widely used for pollutant adsorption as an environmental remediation tool (Gogoi and Pulikkal, 2022, 2024; Gogoi et al., 2024; Gogoi et al., 2025; Saad et al., 2025).

So, currently studies on clay functionalization are still quite common with montmorillonites for various purposes (Asgari and Sundararaj, 2018; Kenawy et al., 2018; Apetrei and Camurlu, 2020; Yilmaz et al., 2020; Pei et al., 2022). However, the possibilities are becoming increasingly broader, with research on saponite (Carniato et al., 2020; Chen et al., 2021; Kenne Dedzo et al., 2021; Marchesi et al., 2021), vermiculite (Ahmed et al., 2020; Ali et al., 2020; Soleimanpour Moghadam et al., 2022), mica/illite (Li et al., 2019; Pazos et al., 2020) and also, to a lesser extent, kaolinite (Detellier, 2018; Dedzo, 2019; Anju and Prasad, 2020; Saikia, 2020). The most common delamination and intercalation methods involve mechanical (Neto et al. de Neto et al., 2021), magnetic stirring (Zaccaron et al., 2025), as well as sonication (Chen et al., 2022).

On the other hand, the mechanical modification of kaolin through high-energy milling has been studied as a way to modify its properties and expand its application possibilities in different industrial sectors (Leonel et al., 2014; Hamzaoui et al., 2015; Bombazaro and Bernardin, 2022).

Although kaolin has been widely used as a mineral filler in polymer matrices in various industrial sectors (Awasthi et al., 2019; Doagou-Rad et al., 2020; Adeniyi et al., 2023), the study of the organic modification of kaolin is important because it is a widely available and low-cost clay, making it an attractive option for many industries. Through organophilization, kaolin can be chemically modified to improve its properties, making it even more versatile and adaptable to different needs. Thus, the objective of this study was to investigate whether the high-energy milling process can act as a potential enhancer in the functionalization of kaolin and which functionalization variables—type of organic molecule, reaction time, and kaolin mass—are most effective in modifying the basal spacing of the kaolin used.

2. Materials and methods

2.1. Kaolin preparation

For this study, a high-purity kaolin was used. The high-energy milling (HEM) process was conducted in a controlled milling to obtain nanometric-scale kaolin ($D_{90} \leq 1$ μm). A MasterMix agitator and a Netzsch Discus 30 horizontal mill were used, with a silicon carbide (SiC) lining and 0.4 mm diameter cerium-stabilized zirconium beads with a density of 3.8 kg (Netzsch Cerabeads), occupying 65 % of the mill volume. To minimize variables, the milling process was carried out using only deionized water, without the addition of any auxiliary additives.

The analysis of oxides present in the kaolin was performed using X-ray fluorescence (XRF), with wavelength dispersive X-ray fluorescence spectrometry (WDXRF, PANalytical AxiosMax). The loss on ignition (L. O.I.) was determined at 1000 °C to help in the impurities identification, accessory minerals, or adulterants that might be present in the kaolin sample.

The mineralogical characterization, both qualitative and quantitative, was conducted by combining X-ray diffraction (XRD) results with Rietveld refinement (Rietveld, 1969). This was done using a Siemens diffractometer (D-5000, Erlangen, Germany) with Cu Kα radiation ($\lambda = 1.5406$ Å), 40 kV acceleration, and 30 mA, covering a 2θ range of 3° to 75° in 0.05°/1 s steps. The TOPAS software, version 5 (Bruker AXS, Karlsruhe, Germany), was used for the Rietveld refinements, using the structural models from ICDD files. Finally, the internal standard method (Riello, 2004; Kern et al., 2012) was used to quantify the amorphous phase, using 15 % ZnO (zinc oxide) with known purity of 99.0 % (from Panreac). The degree of crystallinity, a key factor influencing the intercalation process (Mbey et al., 2020), was evaluated using the Hinckley Index (HI) (Hinckley, 1962), which quantifies both crystallinity and the degree of order/disorder within the kaolinite phase. This index is derived from the d_{110} and d_{111} reflections in the 2θ range of 20°–23°. The HI is calculated by summing the heights of the (111) and (110) reflections relative to the baseline, along with the height of the (110) reflection from the overall baseline. Well-defined and intense reflections indicate a high degree of ordering in the kaolinite phase, while increased disorder leads to a reduction in the number of reflections, along with broadening and decreased intensity, signifying lower crystallinity or greater disorder. HI values greater than 1.0 correspond to high crystallinity or order, values between 0.5 and 0.25 are considered low, and HI values below 0.25 are indicative of very low crystallinity (Aparicio and Galán, 1999). This analysis provides information on the crystalline structure of the raw kaolin and evaluates its behavior after the high-energy milling process, allowing for the assessment of surface modification, diffraction peak shifts or broadening, and the appearance of additional peaks (Sánchez-Soto et al., 2004; Bombazaro and Bernardin, 2022).

Differential thermal analysis (DTA) and thermogravimetric analysis (TGA) of the samples were conducted using a simultaneous analyzer (Netzsch 409 Jupiter F3, Germany), with a heating rate of 10 °C/min from room temperature to 1100 °C in synthetic air, to detect endo or exothermic event temperatures, and possible phase transitions.

Particle size distribution was determined using the sedimentation method (SediGraph III Plus V1.00 analyzer) by gravity, monitored by X-rays; calculations were based on Stokes' law (Stokes, 1844) and Beer's law (Beer, 1852). The analyses were conducted on raw (K_R) and post-milling kaolin (K_{HEM}) samples to assess the evolution of cumulative and class (range) particle size distributions.

Specific surface area was determined by the BET method (Brunauer, Emmett, and Teller) using a Quantachrome Nova 1200e device, with liquid nitrogen as the adsorbate, for both raw (K_R) and post-milling (K_{HEM}) samples. The results complement the particle size distribution and, with the trend of showing a higher surface area compared to untreated kaolinite (K_R), indicate the effectiveness of mechanical activation in increasing the surface area.

Cation exchange capacity (CEC) for determining the total capacity of raw and mechanically altered kaolin to hold exchangeable cations (Chapman, 2016), was carried out using optical emission spectroscopy, identifying Na, K, Ca, and Mg elements. The sum of these elements in meq/100 g was determined after sample preparation by dilution in Milli-Q grade deionized water (Grade I, 0.1 μS/cm at 25 °C). After high-energy milling of kaolinite, CEC can be significantly influenced by changes in specific surface area, particle surface charges, and crystalline microstructure.

Structural differences in kaolin can be detected by spectroscopic methods. Fourier-transform infrared spectroscopy (FTIR), applied to clay mineralogy, lies in its ability to characterize functional groups and the fingerprint region of very small sample quantities (Saikia and Parthasarathy, 2010). This analysis was performed on a Shimadzu IR Prestige-21 device, in powder form by attenuated total reflectance (ATR) directly on the sample. The range evaluated was 400 to 4000 cm^{-1}, with a resolution of 4 cm^{-1} and a speed of 0.2 cm/s.

Microstructural analysis using scanning electron microscopy (SEM) was performed on a Jeol JSM 6390 device, with energy-dispersive spectroscopy (EDS) probe providing the qualitative elemental chemical composition of the sample, to verify the mechanical alteration caused by the HEM process. The samples were gold-coated for analysis.

2.2. Intercalation process

The intercalation process was developed based on the adapted method described by Zhang et al. (2014). To ensure greater reliability, 2^k factorial experiments were also applied (Table 1), altering intercalation variables such as the intercalating molecule, agitation time, and kaolin mass (K_{HEM}). The selected chemical compounds were dimethyl sulfoxide (DMSO, 99.9 %, Synth©, PA-ACS, M.W.:78.13) and diaminomethanal (urea, Dinâmica©, PA-ACS, M.W.: 60.06) as they had shown satisfactory results in previous studies (Paiva et al., 2005; Zhu et al., 2012; Mbey et al., 2013; Elhadj and Perrin, 2021), and are also low-cost and classified as non-toxic. The agitation time varied between 12 and 24 h, and the kaolin (K_{HEM}) powder mass between 10 and 50 g, based on previous studies (Zhang et al., 2017; Makó et al., 2019; Leal et al., 2021). Since these studies showed better intercalation behavior at 60 °C, all experiments were conducted at this temperature.

Initially, solutions of the intercalation agents were prepared in 200 mL glass beakers, with 90 mL of DMSO and 10 mL of deionized water, and 50 g of urea with 50 mL of deionized water. These solutions were used for the kaolin intercalation.

After mixing, the dispersions of the solutions were separated by centrifugation (Excelsa 2 Fanem Centrifuge, model 205 N, at TC3193) for 10 min, washed twice with ethanol (92.3° INPM), and dried in an oven (Gigante brand) at 60 °C for 24 h. The obtained samples were ground in a porcelain mortar and passed through a #325 mesh sieve (45 μm).

Through X-ray diffraction tests, the intensity and position of the peaks were observed to evaluate the basal spacing opening and confirm the effectiveness of the molecular intercalation (Gao et al., 2012). These tests were performed on a Siemens diffractometer (D-5000, Erlangen, Germany), with Cu Kα incident radiation (λ = 1.5406 Å, 40 kV, and 30 mA), 2θ range from 3° to 28°, in 0.05°/1 s steps.

Intercalation typically produces well-defined changes in the X-ray diffraction pattern of kaolinite, easily observed for the 001 reflection, altering the lower diffraction angles due to its characteristic d-spacing value of 7.2 Å, thus allowing the intercalated material to fit (Fafard, 2018).

To evaluate the increase in the basal interplanar distance of the experiments conducted, Bragg's Law was applied, according to Eq. (1) (Bragg and Bragg, 1913).

$$n\lambda = 2d\,sin\theta \quad (1)$$

Where:
d = basal spacing (Å);
θ = angle of incidence relative to the considered plane;
n = diffraction order (1);
λ = wavelength of the incident radiation (Cu Kα = 1.54 Å).

The extent of the reaction, commonly referred to as a ratio known as the "intercalation ratio" (also called the degree of reaction), is estimated using the peak intensity ratio of the modified 001 reflection compared to the intensity of the residual unmodified kaolinite. This was obtained using Eq. (2) (Wiewiora and Brindley, 1969). The ratio assumes the same degree of particle orientation for both the expanded and unexpanded phases (Mbey et al., 2013, 2020).

$$IR = \left(\frac{l_{m(001)}}{l_{m(001)} + l_{o(oo1)}}\right) \times 100 \quad (2)$$

Where:
IR = Intercalation Ratio;
$l_{o(001)}$ = Original residual peak intensity;
$l_{m(001)}$ = Shifted peak intensity observed for the functionalized material.

3. Results and discussion

3.1. Kaolin samples characterization

The chemical analysis of the high-purity kaolin studied (Table 2), compared to a theoretical kaolin, shows values that are quite close. It is important to note that the other oxides present are <1 %, with a variation of little relevance (<0.5 %), associated with the error.

The variation caused by the increase of 0.6 % SiO_2 and 0.7 % in L.O.I., as well as the reduction of 1.7 % Al_2O_3, may be associated with the exposure of aluminol groups (Al-OH) during the milling process.

The mineralogical composition obtained by XRD for the raw kaolin (K_R) and kaolin processed by high-energy milling (K_{HEM}) are present in Fig. 1. The predominant presence of the clay mineral kaolinite (ICDD n. 14–164 $Si_2Al_2O_5(OH)_4$) and traces of illite (ICDD n. 29–0370 $(K,H_3O)(Al, Mg, Fe)_2(Si, Al)_4O_{10}[(OH)_2,(H_2O)]$) can be identified.

The amorphization of mineral crystallinity due to the milling process, associated with the appearance of a halo formed between angles 20 and 30° 2θ, is clearly detected in the K_{HEM} sample, (Derouiche and Baklouti, 2021). According to the Hinckley Index (HI), the crystallinity of the studied samples can be described as high crystallinity for K_R (HI = 1.32) and low crystallinity for K_{HEM} (HI = 0.30).

Table 3 illustrates the quantification obtained by Rietveld, where an increase in the amorphous phase content after milling (+23.44 %) can be observed, indicating the breakdown of the original kaolinite crystalline structure and the formation of an amorphous phase. Consequently, there is a decrease in kaolinite content (−29.11 %), along with

Table 1
Data matrix of the 2^k factorial experimental design for analysis of intercalation parameters.

Experiment	Levels			Factors		
				Molecule	Time (h)	K_{HEM} mass (g)
1	−1	−1	−1	urea	12	10
2	+1	−1	−1	DMSO	12	10
3	−1	+1	−1	urea	24	10
4	+1	+1	−1	DMSO	24	10
5	−1	−1	+1	urea	12	50
6	+1	−1	+1	DMSO	12	50
7	-1	+1	+1	urea	24	50
8	+1	+1	+1	DMSO	24	50
9 (centroid)	-1	0	0	urea	18	30
10 (centroid)	+1	0	0	DMSO	18	30

Table 2
Chemical analysis obtained by X-ray fluorescence (XRF) of raw kaolin (K_R), kaolin processed by high-energy milling (K_{HEM}) and theorical kaolin (according Murray, 2006).

Materials	Oxides (%)			
	SiO_2	Al_2O_3	L.O.I.	other
Theoretical	46.3	39.8	13.9	–
K_R	46.0	39.4	13.7	0.9
K_{HEM}	46.6	37.7	14.4	1.3

L.O.I.: Loss on Ignition (1000 °C).

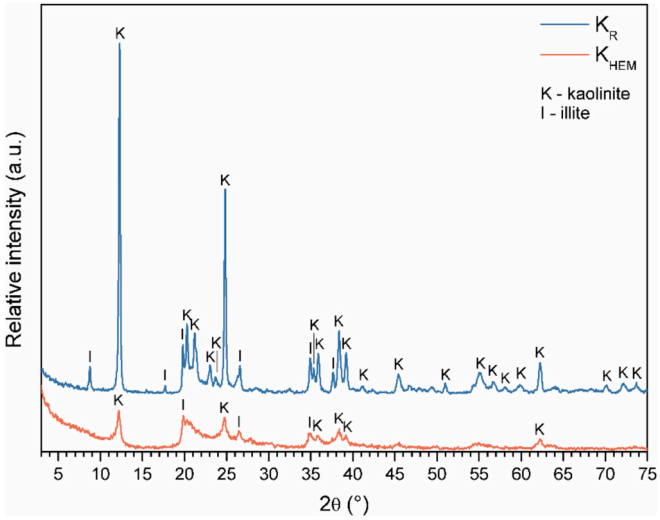

Fig. 1. Mineralogical analysis obtained by XRD of raw kaolin (K_R) and kaolin processed by high-energy milling (K_{HEM}) samples.

Table 3
Mineralogical quantification obtained by Rietveld refinement of raw kaolin (K_R) and kaolin processed by high-energy milling (K_{HEM}) samples.

Phases (%)/Materials	K_R	K_{HEM}
Kaolinite	64.45	35.34
Illite	6.22	11.89
Amorphous phase	29.33	52.77

a noticeable increase in the illite phase (+5.67 %). It is assumed that during the HEM process, the destructuring of kaolinite results in one fraction forming an amorphous phase (metakaolinite) and another fraction becoming illite, which is an intermediate phase characterized by a slightly more disordered mineralogical structure compared to kaolinite. It is worth noting that the amorphization of the material becomes more evident after milling, as observed in the study by Bombazaro and Bernardin (2022).

The thermal analyses in Fig. 2 show a typical curve for kaolinitic clay minerals for K_R (Ptáček et al., 2010; Chakraborty, 2014; Liu et al., 2015). Up to 300 °C, there is a loss of approximately 0.92 % with an endothermic peak at 96.35 °C, associated with the release of surface water (Ilić et al., 2016; Maruoka et al., 2023). Between 300 and 800 °C, there is a loss of 16.50 % with an endothermic peak around 600 °C, which is attributed to the dehydroxylation process of kaolinite (Păcurariu et al., 2017; Tassongwa et al., 2017).

According to the study conducted by Leonel et al. (2014), the high-energy milling process significantly alters the thermal behavior of kaolin, decreasing its thermal stability after the material undergoes the milling process. For K_{HEM}, the release of surface water begins instantly, showing a loss of 3.96 % up to 200 °C with an endothermic peak at 97.4 °C. After the milling process, it exhibited greater thermal stability, with water loss due to the decomposition of hydroxyl groups occurring in a single step around 570 °C, showing a loss of 16.77 % between 200 and 800 °C. It is suggested that, for this loss, the milling process was able to expose the aluminol hydroxyl groups of kaolinite, which were released with less energy (Leonel et al., 2014). Within this range, an endothermic peak at 566.89 °C was also observed, which may be associated with the dehydroxylation of kaolinite and the formation of metakaolin (Sahnoune et al., 2012; Katayama et al., 2014; Guatame-García et al., 2018; Maruoka et al., 2023). Correlating the X-ray diffraction data with the thermal analysis, the mass loss in the temperature range of 200–500 °C, which, as mentioned earlier, may be attributed to the premature dehydroxylation of OH groups in partially disordered kaolinite, presents characteristics similar to illite (Marsh et al., 2018).

Finally, an exothermic peak at 980 °C, present in both samples, is related to the metakaolin crystallization into a new phase, commonly referred as mullite I (Stone, 1952; Comin et al., 2021). The intensity of this peak was lower for K_{HEM}, suggesting that the metakaolin is more disordered and, therefore, lower mullite I crystallization degree.

The particle size distributions (Fig. 3) and average diameters (Table 4) present the results of the milling of the studied kaolin (K_R). This analysis demonstrates the effectiveness of the mechanical process, reducing the material's granulometry to $D_{90} < 1$ μm, with an 11.5× reduction after milling.

It was observed that high-energy milling contributed to refining the size distribution and morphology of kaolin. The material <1 μm increased from <9 % to >90 %, reducing the average diameter by approximately 83 %. It is also important to highlight that the mechanical activation process tends to lead to the kaolin amorphization (Őze and Makó, 2023), as observed in the X-ray diffraction (Fig. 1).

The determination of the specific surface area (Table 5) shows a significant increase after the milling process, rising from 8 to 145 m^2/g, an increase of about 18×, a fundamental characteristic for the intercalation functionalization process.

It is noteworthy that the specific surface area values for kaolinite are commonly between ~10 and 50 m^2/g (Uehara and Gillman, 1981; Yong et al., 1992), and these values can significantly influence the

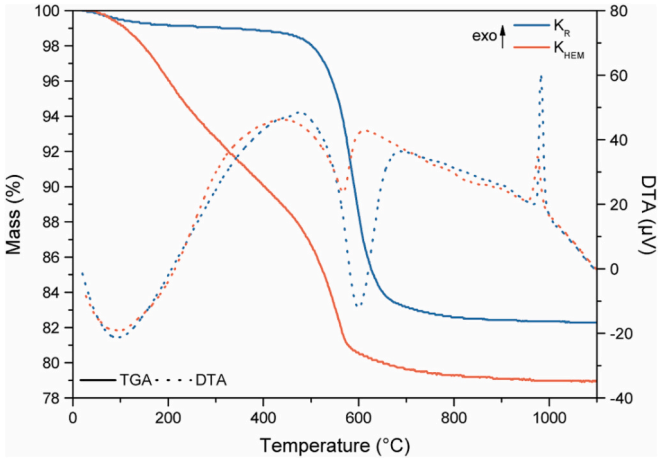

Fig. 2. Thermogravimetric analysis (TGA) and differential thermal analysis (DTA) of raw kaolin (K_R) and kaolin processed by high-energy milling (K_{HEM}) samples.

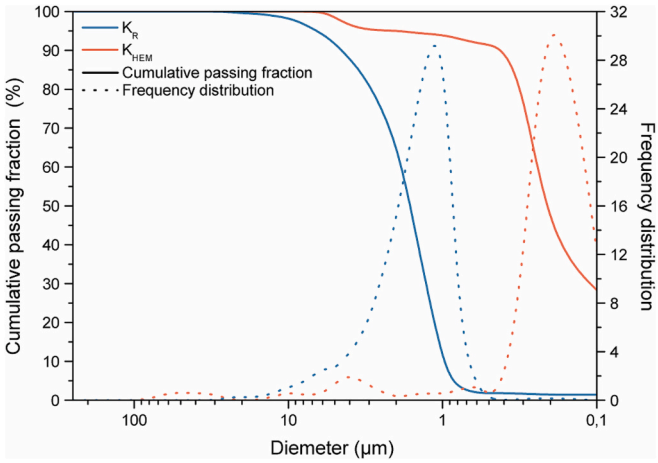

Fig. 3. Particle size distribution of raw kaolin (K_R) and kaolin processed by high-energy milling (K_{HEM}) samples.

Table 4
Granulometric distribution and average particle diameter of raw kaolin (K_R) and kaolin processed by high-energy milling (K_{HEM}) samples.

Materials	D_{90} (μm)	D_{50} (μm)	D_{20} (μm)	D_{10} (μm)	$D_{average}$ (μm)	% < 10	% < 1
K_R	4.49	1.60	1.18	1.02	1.10	98	9
K_{HEM}	0.39	0.22	0.18	0.18	0.18	100	94

Table 5
Specific surface area results of raw kaolin (K_R) and kaolin processed by high-energy milling (K_{HEM}) samples.

Materials	K_R	K_{HEM}
Specific surface area (m^2/g)	8	145

functionalization of clays, providing more sites for interaction with functional molecules. A larger specific surface area allows for greater contact between the clay and the functionalizing agents, increasing the efficiency of the functionalization process. A larger surface area can lead to better adsorption properties, stability, and resistance of the functionalized clay suspensions. Furthermore, it may facilitate the formation of three-dimensional networks and greater aggregation, which are decisive aspects for improving the rheological properties of the clay (Mohammed et al., 2021; Khan et al., 2023; Sarkar et al., 2023).

The values for the cation exchange capacity (CEC) of the K_R and K_{HEM} samples (Table 6) indicate an increase from 0.56 to 4.64 meq/100 g after milling. The CEC of kaolinite strongly depends on the particle size, thickness, and diameter (in the 001 plane), as well as the pH value (Yong et al., 1992; Mitchell and Soga, 2005), with these potentiometric charges increasing as the kaolinite diameter decreases (Chi and Eggleton, 1999).

Hydroxyl groups exposed along the alumina faces of kaolinite may also be able to exchange H^+ ions for some cations. The total alumina face charges are higher when the number of kaolinite layers linked together is smaller. Additionally, a permanently negative charge along the silica faces may result in the substitution of Al^{3+} ions with Si^{4+} ions within the crystal lattice (Chi and Eggleton, 1999; Coles and Yong, 2002), although this source of charge is considered minimal (Bohn et al., 1985). In a previous study on HEM in kaolin, Bombazaro and Bernardin (2022) suggest that the change in CEC may be due to the release of Na^+, Mg^{2+}, and Ca^{2+} ions with the mineral deconstruction of the clay phase during milling. It is important to note that typical CEC values for kaolinite reach up to 15 meq/100 g (Grim, 1968; Coles and Yong, 2002; Hussin et al., 2018). The purity of the material studied may be associated with a low CEC compared to the natural variation of kaolinite, not indicating any detectable isomorphic substitution (Chi and Eggleton, 1999).

The Fourier Transform Infrared (FTIR) spectrum of the kaolin samples studied (Fig. 4) illustrates the bands and the degree of absorbance, with the possible influence of milling. It is important to note that a typical kaolin spectrum shows four bands at 3697, 3669, 3645, and 3620 cm^{-1} (Saikia and Parthasarathy, 2010), and when these characteristic bands are well-defined, the kaolinite structure is ordered. However, when the band at 3669 cm^{-1} disappears, the kaolinite structure becomes disordered and more easily dehydrated (Bich, 2005).

In both K_R and K_{HEM}, bands around 3669 and 3620 cm^{-1} were observed, which may be associated with stretching vibrations of

Table 6
Cation exchange capacity (CEC) analysis of raw kaolin (K_R) and kaolin processed by high-energy milling (K_{HEM}) samples.

Materials	Cation exchange capacity (meq/100 g)				
	CEC Na^+	CEC K^+	CEC Ca^{2+}	CEC Mg^{2+}	CEC Total
K_R	0.20	0.06	0.10	0.20	0.56
K_{HEM}	1.98	1.18	0.86	0.63	4.64

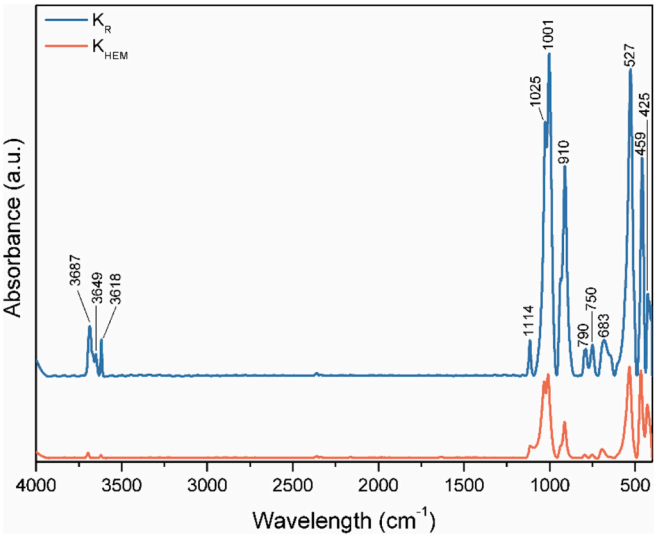

Fig. 4. FTIR analysis of raw kaolin (K_R) and kaolin processed by high-energy milling (K_{HEM}) samples.

hydroxyl (OH) groups. The intensity and specific wavenumber of these bands can provide information about the concentration and environment of the hydroxyl groups in the analyzed material (Tironi et al., 2012).

In the context of clay minerals, the Al-O-H stretching vibration is observed in the range of 1200–700 cm^{-1} (Jozanikohan and Abarghooei, 2022). Thus, the band observed around ~1030 cm^{-1} may be attributed to interference related to the stretching vibrations of silicon-oxygen (Si—O) bonds, while the band observed in the 914–936 cm^{-1} range corresponds to Al-OH bending vibrations, as well as intertetrahedral Si-O-Si bonds in SiO_2 between 780 and 798 cm^{-1}. Finally, the absorbance bands between 430 and 530 cm^{-1} may be associated with Si—O bending and Al-O-Si bending vibrations (Diko et al., 2015).

It is clearly observable that there was a reduction in the absorbance degree after the milling process. The literature (Liang et al., 2023) provides evidence that mechanical alteration can modify the structure and composition of kaolin, leading to a reduction in the absorption degree. Therefore, it is believed that the amorphization achieved by high-energy milling influenced the infrared spectrum, causing changes in the stretching bands of the hydroxyl O—H (Derouiche and Baklouti, 2021). Studies conducted some time ago (Hlavay, 1978; Aglietti et al., 1986) describe that OH groups are irreversibly displaced during mechanical processing, as observed in the thermal analysis (Fig. 2). Therefore, as illustrated by Hamzaoui et al. (2015), the peaks recognized in the stretching region decrease sharply in intensity during the milling process, indicating the cleavage of the simple O—H bonds.

The micrographs obtained by Scanning Electron Microscopy (SEM) of K_R and K_{HEM} are presented in Fig. 5. It is observed that plate-like particles resulting from the lamellar structure of kaolinite crystals are dominant in K_R. The morphology of kaolin particles changed with the milling process, as the SEM image of K_{HEM} shows agglomerated particles, possibly formed by the delamination of the kaolinite structure, making them more rounded and smaller (Fig. 5b). The literature (Őze and Makó, 2023) illustrates that with prolonged milling, coalescence and agglomeration are more prevalent than particle fracture, so a significant fraction of the particles becomes aggregates with porous surfaces.

The mechanical activation caused the delamination of kaolinite and, therefore, the breakdown of its structure. It is also emphasized that the delamination process occurs with localized heating (Derouiche and Baklouti, 2021), resulting in partial dehydroxylation. After the combination of OH units, the formed water adsorbs and coordinates the highly

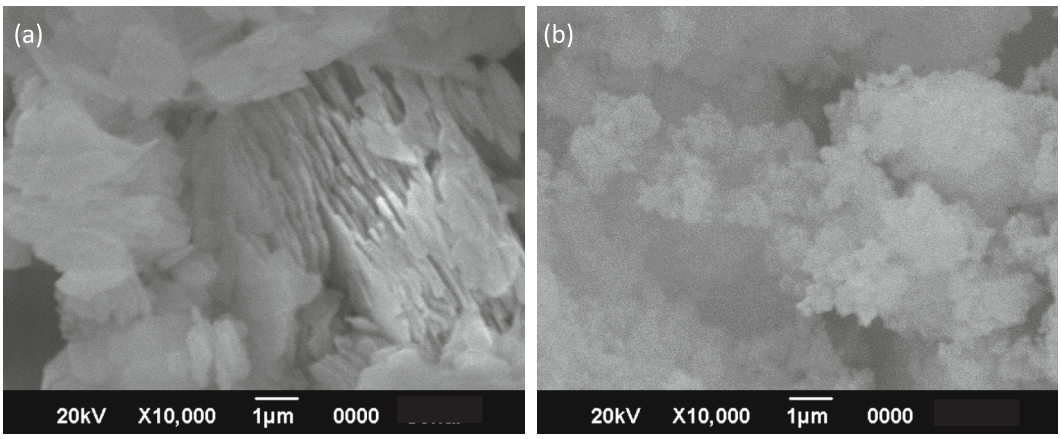

Fig. 5. Micrographs obtained by scanning electron microscopy (SEM) of (a) raw kaolin (K_R) and (b) kaolin processed by high-energy milling (K_{HEM}) samples.

surfactant sites of the delaminated kaolinite, increasing the effective solubility of organic compounds, of which the spherical shape of the particles was a result of adsorption at the interface between immiscible phases (Gonzalez Garcia et al., 1991).

The micrographs and EDS spectrum (Fig. 6) show that the K_R appears more dispersed compared to the agglomerated K_{HEM}, as a result of the high-energy milling process. The same behavior can be observed for both samples, with the presence of Al + Si, the key elements of kaolinite, with similar peak intensities.

3.2. Characterization of K_{HEM}-intercalated with Urea and DMSO

Fig. 7 illustrates the mineralogical analyses by X-ray diffraction of the experiments conducted on K_{HEM}, intercalated with urea (a and b) and with DMSO (c and d). As discussed previously, the milling process amorphized the material, which is also evident in these diffractograms. In Fig. 7(a), the appearance of new peaks is possibly associated with the presence of urea, which does not occur in the DMSO intercalation (Fig. 7 (c)). It should be noted that urea is a crystalline organic compound.

Fig. 7(b and d) illustrate more specifically the shift of the $d_{(001)}$ peaks of kaolinite for both intercalating molecules (urea and DMSO). It becomes evident that, even with lower intensity, peak shifts occurred, indicating that intercalation took place with HEM for the functionalized materials. The residual peaks at around ~12.3° 2θ can be related to the fractions of kaolin that were not intercalated.

Table 7 shows the values found for the increase in basal spacing (d) from the experiments that occurred through peak shifting, as well as the intercalation ratio (IR) content. Originally, kaolinite exhibits a basal spacing of $d = 7.2$ Å, and the milling process did not alter this condition.

For the intercalation of the molecules, the increase in the basal

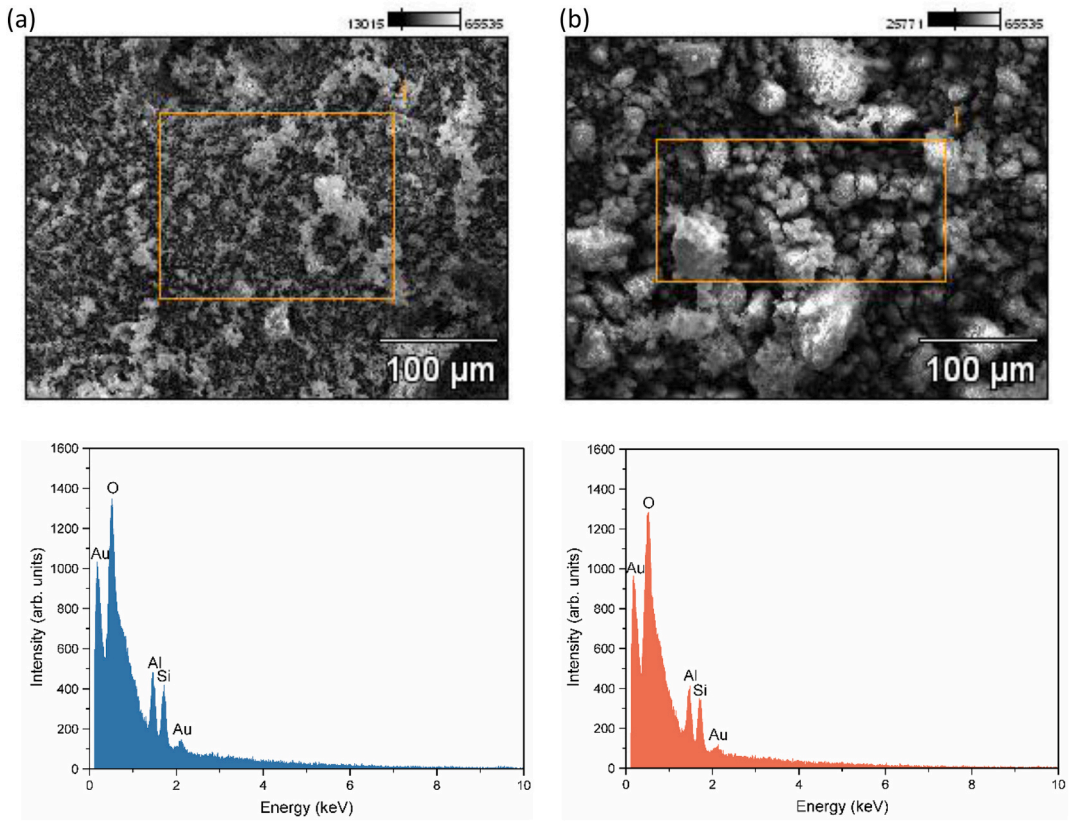

Fig. 6. Micrographs and energy-dispersive spectroscopy (EDS) spectrum of (a) raw kaolin (K_R) and (b) kaolin processed by high-energy milling (K_{HEM}) samples.

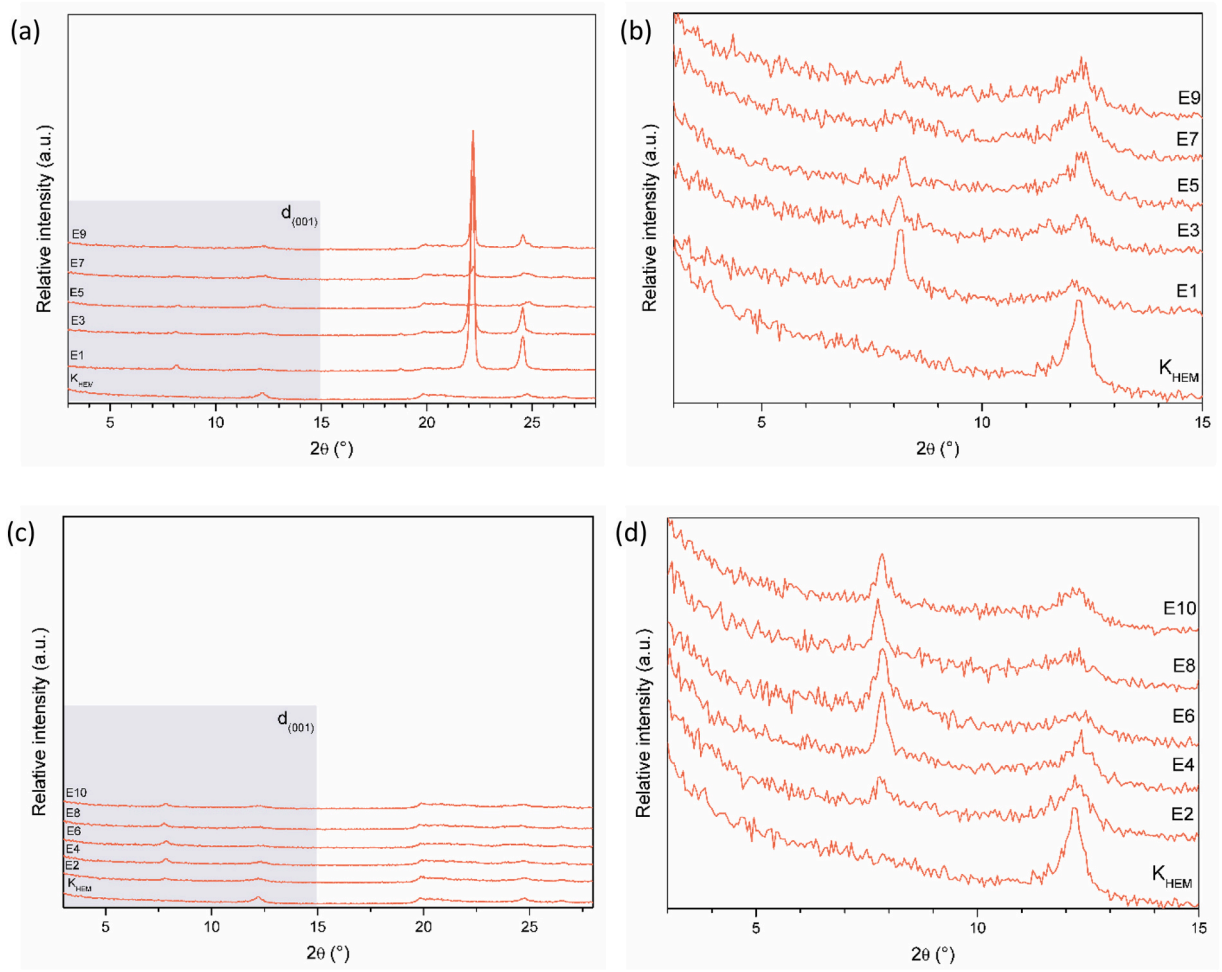

Fig. 7. Mineralogical analysis of the experiments conducted on kaolin processed by high-energy milling (K_{HEM}) intercalated with (a and b) urea and (c and d) DMSO.

Table 7
Basal spacing (*d*) and intercalation ratio (*IR*) of the experiments performed on kaolin processed by high-energy milling (K_{HEM}).

Experiment	*d* (Å)	*IR* (%)
E1	10.9	9.43
E2	11.3	7.32
E3	10.9	7.23
E4	11.3	10.54
E5	10.7	6.34
E6	11.3	10.29
E7	10.7	6.24
E8	11.4	9.90
E9	10.9	6.99
E10	11.3	8.96

spacing of kaolinite was from 7.2 Å to ~10.8 Å with urea and to ~11.3 Å with DMSO. These values were also observed in studies by Zhang et al. (2017), Seifi et al. (2016), Mahdavi et al. (2014), Valášková et al. (2007) and Makó et al. (2009) for urea, and Zhang et al. (2015), Mbey et al. (2020), Fang et al. (2005), (Mbey et al., 2013), de Macêdo Neto et al. (2023) and de Faria et al. (2009) for DMSO.

The calculated intercalation rates were < 10 %, and several factors may be linked to this, where for samples with the same granulometry, the preparation conditions likely determine the intercalation ratios (Mbey et al., 2013), also related to the material's crystallinity (Mbey et al., 2020). It is clear that amorphization has a direct impact on the intercalation of organic molecules, affecting the effectiveness of this step, being proven as one of the factors that influence the degree of intercalation (Franco and Ruiz Cruz, 2004).

4. Conclusion

The milling process effectively altered the structure of the kaolin studied. In the particle size distribution analysis, the D_{90} of the studied samples decreased from 4.49 μm (K_R) to 0.39 μm (K_{HEM}), reaching values ≤1 μm as expected after high-energy milling (HEM). This process increased the specific surface area of the studied solid more than 18 times, from 8 to 145 m^2/g. The structural breakdown altered the material's crystallinity, making it more amorphous, as observed in the X-ray diffraction analysis. Similarly, in the morphology, the traditional plate-like structure of the clay disappeared, giving way to agglomerates, despite energy dispersive spectroscopy showing the same presence of Si + Al on the material's surface. Through phase quantification by Rietveld, it was observed that the amorphous phase content increased (~23 %) with the mechanical milling treatment, while the kaolinite phase content decreased (~29 %). Another significant factor was the increase in the illite phase (~5 %), formed from the HEM transition of a fraction of kaolinite into illite and another into the amorphous phase (metakaolinite). It is important to highlight that illite can be considered mineralogically as an intermediate phase formed from kaolinite's structural breakdown by HEM. This hypothesis is aligned with the changes observed in the thermogravimetric analysis (TG) curve of the K_{HEM} sample, particularly the significant mass loss between 200 and 500 °C, which could be attributed to the early release of water (OH groups) from partially deconstructed kaolinite, resembling illite in the X-ray diffraction analysis. The structural breakdown of the kaolin was also

evident in the FTIR test, with the minimization of intensity in the OH group bands, which were irreversibly shifted during the mechanical processing, and in the thermal analysis, which showed the instant mass loss.

Further analysis by X-ray diffraction revealed that the shift of the 001 peak of kaolinite on the 2θ axis indicated that organic intercalation did indeed occur, aiming to increase the basal spacing (*d*) of the experiment, which is the main objective of organofilization. Kaolinite, which naturally has a *d* of 7.2 Å, reached a *d* of ~10.8 Å (urea) and ~ 11.3 Å (DMSO) after the intercalation experiments, values commonly found in the literature. These results were obtained between 12 and 24 h, contrasting with the typical period of 48 h to 7 days reported in the literature. Interestingly, these results were not influenced by the milling process, where it was proven that HEM was not a determining factor in assisting basal spacing (*d*) opening.

For evaluating the intensity of the kaolinite 001 peaks, the intercalation ratio (*IR*) was obtained, which revealed the percentage of organic molecule intercalation on the surface of the kaolin studied. Intercalation rates of <10 % were observed for K_{HEM} with *IR*, effectively intercalated or inserted into the interlayer spaces of the clay minerals during the organofilization process. It is evident that kaolinite amorphization directly impacted the amount of organic molecules introduced into the experiment. However, considering the fact that the *d* reached values similar to other studies, it is assumed that kaolinite with a higher specific surface area, and consequently higher reactivity, required a lower intercalation rate to achieve the same result as highly ordered kaolinite.

CRediT authorship contribution statement

Alexandre Zaccaron: Writing – original draft, Visualization, Validation, Project administration, Methodology, Investigation, Funding acquisition, Data curation. **Fabiano Raupp-Pereira:** Writing – review & editing, Validation, Formal analysis. **Vitor de Souza Nandi:** Writing – original draft. **João C.C. Abrantes:** Writing – review & editing, Validation, Formal analysis. **Manuel J. Ribeiro:** Writing – original draft, Validation, Formal analysis. **Adriano Michael Bernardin:** Supervision, Resources, Methodology, Formal analysis, Conceptualization.

Declaration of competing interest

The authors declare that they have no conflict of interest.

Acknowledgments

The authors are grateful to the Coordination for Higher Education Improvement (CAPES/Brazil) process no. 88887.502321/2020-00.

Data availability

No data was used for the research described in the article.

References

Adeniyi, A.G., Iwuozor, K.O., Emenike, E.C., 2023. Material development potential of Nigeria's Kaolin. Chem. Afr. https://doi.org/10.1007/s42250-023-00642-2.

Aglietti, E.F., Porto Lopez, J.M., Pereira, E., 1986. Mechanochemical effects in kaolinite grinding. I. Textural and physicochemical aspects. Int. J. Miner. Process. 16, 125–133. https://doi.org/10.1016/0301-7516(86)90079-7.

Ahmed, Z., Wu, P., Jiang, L., Liu, J., Ye, Q., Yang, Q., Zhu, N., 2020. Enhanced simultaneous adsorption of Cd(II) and Pb(II) on octylamine functionalized vermiculite. Colloids Surfaces A Physicochem. Eng. Asp. 604, 125285. https://doi.org/10.1016/j.colsurfa.2020.125285.

Ali, N., Ali, F., Farooq, R., Said, A., Saeed, S., Bilal, M., 2020. Photo-oxidative degradation of organo-functionalized vermiculite clay-reinforced polyimide composites. Appl. Nanosci. 10, 3725–3733. https://doi.org/10.1007/s13204-020-01514-8.

Anju, P., Prasad, V.S., 2020. Functionalization-induced self-assembly of polystyrene/kaolinite in situ nanocomposites into giant vesicles. Langmuir 36, 1761–1767. https://doi.org/10.1021/acs.langmuir.9b03996.

Aparicio, P., Galán, E., 1999. Mineralogical interference on kaolinite crystallinity index measurements. Clay Clay Miner. 47, 12–27. https://doi.org/10.1346/CCMN.1999.0470102.

Apetrei, R.-M., Camurlu, P., 2020. The effect of montmorillonite functionalization on the performance of glucose biosensors based on composite montmorillonite/PAN nanofibers. Electrochim. Acta 353, 136484. https://doi.org/10.1016/j.electacta.2020.136484.

Asgari, M., Sundararaj, U., 2018. Silane functionalization of sodium montmorillonite nanoclay: the effect of dispersing media on intercalation and chemical grafting. Appl. Clay Sci. 153, 228–238. https://doi.org/10.1016/j.clay.2017.12.020.

Awasthi, A., Jadhao, P., Kumari, K., 2019. Clay nano-adsorbent: structures, applications and mechanism for water treatment. SN Appl. Sci. 1, 1076. https://doi.org/10.1007/s42452-019-0858-9.

Beer, A., 1852. Bestimmung der absorption des rothen Lichts in farbigen flüssigkeiten. Ann. Phys. 162, 78–88. https://doi.org/10.1002/andp.18521620505.

Bich, C., 2005. Contribution à L'étude de L'activation Thermique du Kaolin : Évolution de la Structure Cristallographique et Activité Pouzzolanique. Institut National des Sciences Appliqués de Lyon, Lyon, France.

Bohn, H., McNeal, B., O'Connor, G., 1985. Soil Chemistry. Williams & Wilkins, New York, USA.

Bombazaro, J.L., Bernardin, A.M., 2022. Improving plasticity of kaolins by high-energy milling for use in porcelain tile compositions. Open Ceram. 10, 100256. https://doi.org/10.1016/j.oceram.2022.100256.

Bragg, W.H., Bragg, W.L., 1913. The reflection of X-rays by crystals. Proc. R. Soc. London. Ser. A Contain. Pap. a Math. Phys. Character 88, 428–438.

Carniato, F., Gatti, G., Bisio, C., 2020. An overview of the recent synthesis and functionalization methods of saponite clay. New J. Chem. 44, 9969–9980. https://doi.org/10.1039/D0NJ00253D.

Chakraborty, A.K., 2014. Thermal methods. In: Chakraborty, Akshoy Kumar (Ed.), Phase Transformation of Kaolinite Clay. Springer India, New Delhi, pp. 15–42. https://doi.org/10.1007/978-81-322-1154-9_3.

Chapman, H.D., 2016. Cation-exchange capacity. In: Black, C.A., Evans, D.D., White, J.L., Ensminger, L.E., Clark, F.E. (Eds.), Methods of Soil Analysis: Part 1. American Society of Agronomy, Ankeny, Iowa, pp. 891–901. https://doi.org/10.2134/agronmonogr9.2.c6.

Chen, D., Luo, D., Zhen, W., Zhao, L., 2021. Effect of functionalized organic saponite on performance, crystallization and rheology of poly (lactic acid). Appl. Clay Sci. 207, 106091. https://doi.org/10.1016/j.clay.2021.106091.

Chen, X., Tremblay, A.Y., Fauteux-Lefebvre, C., 2022. Controlled kaolinite delamination in urea and surfactant solutions using high-power ultrasonication: impact on platelet morphologies. Appl. Clay Sci. 228, 106640. https://doi.org/10.1016/j.clay.2022.106640.

Chi, M., Eggleton, R.A., 1999. Cation exchange capacity of kaolinite. Clay Clay Miner. 47, 174–180. https://doi.org/10.1346/CCMN.1999.0470207.

Coles, C.A., Yong, R.N., 2002. Aspects of kaolinite characterization and retention of Pb and Cd. Appl. Clay Sci. 22, 39–45. https://doi.org/10.1016/S0169-1317(02)00110-2.

Comin, A.B., Zaccaron, A., de Souza Nandi, V., Inocente, J.M., Muller, T.G., Dal Bó, A.G., Bernardin, A.M., Peterson, M., 2021. Measurement of apparent sintering activation energy for densification of clays. Clay Miner. 56, 299–305. https://doi.org/10.1180/clm.2022.11.

da Silva Favero, J., dos Santos, V., Weiss-Angeli, V., Gomes, L.B., Veras, D.G., Dani, N., Mexias, A.S., Bergmann, C.P., 2019. Evaluation and characterization of Melo Bentonite clay for cosmetic applications. Appl. Clay Sci. 175, 40–46. https://doi.org/10.1016/j.clay.2019.04.004.

de Faria, E.H., Lima, O.J., Ciuffi, K.J., Nassar, E.J., Vicente, M.A., Trujillano, R., Calefi, P. S., 2009. Hybrid materials prepared by interlayer functionalization of kaolinite with pyridine-carboxylic acids. J. Colloid Interface Sci. 335, 210–215. https://doi.org/10.1016/j.jcis.2009.03.067.

de Macêdo Neto, J.C., de Freitas, B.M., de Miranda, A.G., de Almeida Rodrigues, R., Del Pino, G.G., Kieling, A.C., dos Santos, M.D., Duvoisin Junior, S., Sanches, A.E., Gondres Torné, I., Silva, C.C., da Costa, J.C.M., Bello, R.H., 2023. The stability and properties of polystyrene/kaolinite nanocomposites during synthesis via emulsion polymerization. Polymers (Basel) 15, 2094. https://doi.org/10.3390/polym15092094.

de Neto, J.C.M., do Nascimento, N.R., Bello, R.H., de Verçosa, L.A., Neto, J.E., da Costa, J.C.M., Diaz, F.R.V., 2021. Kaolinite review: intercalation and production of polymer nanocomposites. Eng. Sci. 17, 28–44. https://doi.org/10.30919/es8d499.

de Oliveira, C.I.R., Rocha, M.C.G., de Assis, J.T., Verly, J., da Silva, A.L.N., Bertolino, L. C., 2018. Desenvolvimento de nanocompósitos de polipropileno/argila bentonítica organofílica. In: Abdala, M.R.W.S. (Ed.), Ciência e Engenharia de Materiais - Vol 4. Atena Editora, Ponta Grossa, pp. 108–122. https://doi.org/10.22533/at.ed.642182910.

de Paiva, L.B., Morales, A.R., Díaz, F.R.V., 2008. Argilas organofílicas: características, metodologias de preparação, compostos de intercalação e técnicas de caracterização. Cerâmica 54, 213–226. https://doi.org/10.1590/S0366-69132008000200012.

de Santos, P.S., 1989. Ciências e tecnologia de argilas, 2a. ed. Edgard Blücher Ltda, São Paulo, SP.

Dedzo, G.K., 2019. Kaolinite clay mineral reactivity improvement through ionic liquid functionalization. Isr. J. Chem. 59, 778–788. https://doi.org/10.1002/ijch.201800130.

Derouiche, R., Baklouti, S., 2021. Phosphoric acid based geopolymerization: effect of the mechanochemical and the thermal activation of the kaolin. Ceram. Int. 47, 13446–13456. https://doi.org/10.1016/j.ceramint.2021.01.203.

Detellier, C., 2018. Functional Kaolinite. Chem. Rec. 18, 868–877. https://doi.org/10.1002/tcr.201700072.

Diko, M., Ekosse, G., Ogola, J., 2015. Fourier transform infrared spectroscopy and thermal analyses of kaolinitic clays from South Africa and Cameroon. Acta Geodyn. Geomater. 13, 149–158. https://doi.org/10.13168/AGG.2015.0052.
Doagou-Rad, S., Islam, A., Merca, T.D., 2020. An application-oriented roadmap to select polymeric nanocomposites for advanced applications: a review. Polym. Compos. 41, 1153–1189. https://doi.org/10.1002/pc.25461.
Elhadj, M.-S.Y., Perrin, F.X., 2021. Influencing parameters of mechanochemical intercalation of kaolinite with urea. Appl. Clay Sci. 213, 106250. https://doi.org/10.1016/j.clay.2021.106250.
Fafard, J., 2018. Functionalized Materials Based on the Clay Mineral Kaolinite. University of Ottawa, Ottawa, Ontario.
Fang, Q., Huang, S., Wang, W., 2005. Intercalation of dimethyl sulphoxide in kaolinite: molecular dynamics simulation study. Chem. Phys. Lett. 411, 233–237. https://doi.org/10.1016/j.cplett.2005.06.052.
Franco, F., Ruiz Cruz, M.D., 2004. Factors influencing the intercalation degree ('reactivity') of kaolin minerals with potassium acetate, formamide, dimethylsulphoxide and hydrazine. Clay Miner. 39, 193–205. https://doi.org/10.1180/0009855043920130.
Gao, F., 2004. Clay/polymer composites: the story. Mater. Today 7, 50–55. https://doi.org/10.1016/S1369-7021(04)00509-7.
Gao, X., Mao, H., Lu, M., Yang, J., Li, B., 2012. Facile synthesis route to NiO–SiO2 intercalated clay with ordered porous structure: intragallery interfacially controlled functionalization using nickel–ammonia complex for deep desulfurization. Microporous Mesoporous Mater. 148, 25–33. https://doi.org/10.1016/j.micromeso.2011.07.022.
Gogoi, A.J., Pulikkal, A.K., 2022. Clay–gemini surfactant hybrid materials for elimination of inorganic pollutants: a comprehensive review. Results Chem. 4, 100586. https://doi.org/10.1016/j.rechem.2022.100586.
Gogoi, A.J., Pulikkal, A.K., 2024. Propane-1,3-bis(hexadecyldimethylammonium bromide)-bentonite-based novel hybrid material for the elimination of textile dyes. J. Mol. Liq. 395, 123890. https://doi.org/10.1016/j.molliq.2023.123890.
Gogoi, A., Anjudikkal, J., Pulikkal, A.K., Kumar, D., 2024. Discharging of tetracycline antibiotic effluents from the aqueous phase using gemini–clay hybrid material. Next Res. 1, 100031. https://doi.org/10.1016/j.nexres.2024.100031.
Gogoi, A., Anjudikkal, J., Pulikkal, A.K., 2025. Adsorption, antibacterial and molecular dynamic studies of bentonite clay–gemini (Bt–16-4-16) hybrid material. J. Water Process Eng. 69, 106602. https://doi.org/10.1016/j.jwpe.2024.106602.
Gonzalez Garcia, F., Ruiz Abrio, M.T., Gonzalez Rodriguez, M., 1991. Effects of dry grinding on two kaolins of different degrees of crystallinity. Clay Miner. 26, 549–565. https://doi.org/10.1180/claymin.1991.026.4.09.
Grim, R.E., 1968. Clay Mineralogy, 2nd ed. McGraw-Hill, New York, NY.
Guatame-García, A., Buxton, M., Deon, F., Lievens, C., Hecker, C., 2018. Toward an on-line characterization of kaolin calcination process using short-wave infrared spectroscopy. Miner. Process. Extr. Metall. Rev. 39, 420–431. https://doi.org/10.1080/08827508.2018.1459617.
Hamzaoui, R., Muslim, F., Guessasma, S., Bennabi, A., Guillin, J., 2015. Structural and thermal behavior of proclay kaolinite using high energy ball milling process. Powder Technol. 271, 228–237. https://doi.org/10.1016/j.powtec.2014.11.018.
Hinckley, D.N., 1962. Variability in "crystallinity" values among the kaolin deposits of the coastal plain of georgia and South Carolina. Clay Clay Miner. 11, 229–235. https://doi.org/10.1346/CCMN.1962.0110122.
Hlavay, J., 1978. Characterization of the particle size and the crystallinity of certain minerals by IR spectrophotometry and other instrumental methods—II. Investigations on Quartz and Feldspar. Clay Clay Miner. 26, 139–143. https://doi.org/10.1346/CCMN.1978.0260209.
Hussin, A., Rahman, A.H.A., Ibrahim, K.Z., 2018. Mineralogy and geochemistry of clays from Malaysia and its industrial application. IOP Conf. Ser. Earth Environ. Sci. 212, 012040. https://doi.org/10.1088/1755-1315/212/1/012040.
Ilić, B., Radonjanin, V., Malešev, M., Zdujić, M., Mitrović, A., 2016. Effects of mechanical and thermal activation on pozzolanic activity of kaolin containing mica. Appl. Clay Sci. 123, 173–181. https://doi.org/10.1016/j.clay.2016.01.029.
Jozanikohan, G., Abarghooei, M.N., 2022. The Fourier transform infrared spectroscopy (FTIR) analysis for the clay mineralogy studies in a clastic reservoir. J. Pet. Explor. Prod. Technol. 12, 2093–2106. https://doi.org/10.1007/s13202-021-01449-y.
Katayama, M., Kawai, Y., Mizuno, Y., Mizuno, K., Aoyama, M., Kobayashi, Y., 2014. Preparation of dense mullite polycrystals by reaction sintering of kaolin materials and alumina and their microstructure. J. Ceram. Soc. Japan 122, 300–306. https://doi.org/10.2109/jcersj2.122.300.
Kenawy, E.-R., Ghfar, A.A., Wabaidur, S.M., Khan, M.A., Siddiqui, M.R., Alothman, Z.A., Alqadami, A.A., Hamid, M., 2018. Cetyltrimethylammonium bromide intercalated and branched polyhydroxystyrene functionalized montmorillonite clay to sequester cationic dyes. J. Environ. Manag. 219, 285–293. https://doi.org/10.1016/j.jenvman.2018.04.121.
Kenne Dedzo, G., Rigolet, S., Josien, L., Ngameni, E., Dzene, L., 2021. Functionalization of synthetic saponite: Identification of grafting sites and application for anions sequestration. Appl. Surf. Sci. 567, 150911. https://doi.org/10.1016/j.apsusc.2021.150911.
Kern, A., Madsen, I.C., Scarlett, N.V.Y., 2012. Quantifying amorphous phases. In: Kolb, U., Shankland, K., Meshi, L., Avilov, A., David, W. (Eds.), Uniting Electron Crystallography and Powder Diffraction. NATO Science for Peace and Security Series B: Physics and Biophysics. Springer, Dordrecht, pp. 219–231. https://doi.org/10.1007/978-94-007-5580-2_20.
Khan, A., Asiri, A.M., Jawaid, M., Saba, N., Inamuddin, 2020. Effect of cellulose nano fibers and nano clays on the mechanical, morphological, thermal and dynamic mechanical performance of kenaf/epoxy composites. Carbohydr. Polym. 239, 116248. https://doi.org/10.1016/j.carbpol.2020.116248.
Khan, S., Ajmal, S., Hussain, T., Rahman, M.U., 2023. Clay-based materials for enhanced water treatment: adsorption mechanisms, challenges, and future directions. J. Umm Al-Qura Univ. Appl. Sci. https://doi.org/10.1007/s43994-023-00083-0.
Leal, P.V.B., Pereira, D.H., Papini, R.M., Magriotis, Z.M., 2021. Effect of dimethyl sulfoxide intercalation into kaolinite on etheramine adsorption: experimental and theoretical investigation. J. Environ. Chem. Eng. 9, 105503. https://doi.org/10.1016/j.jece.2021.105503.
Leonel, E.C., Nassar, E.J., Ciuffi, K.J., dos Reis, M.J., Calefi, P.S., 2014. Effect of high-energy ball milling in the structural and textural properties of kaolinite. Cerâmica 60, 267–272. https://doi.org/10.1590/S0366-69132014000200016.
Li, Z., Pan, Z., Wang, Y., 2019. Enhanced adsorption of cationic Pb(II) and anionic Cr(VI) ions in aqueous solution by amino-modified nano-sized illite-smectite clay. Environ. Sci. Pollut. Res. 26, 11126–11139. https://doi.org/10.1007/s11356-019-04447-0.
Liang, X., Li, Q., Fang, Y., 2023. Preparation and characterization of modified kaolin by a mechanochemical method. Materials (Basel) 16, 3099. https://doi.org/10.3390/ma16083099.
Liu, Xiaoxu, Liu, Xiaowen, Hu, Y., 2015. Investigation of the thermal behaviour and decomposition kinetics of kaolinite. Clay Miner. 50, 199–209. https://doi.org/10.1180/claymin.2015.050.2.04.
Mahdavi, F., Abdul, R., Khanif, Y., 2014. Intercalation of urea into kaolinite for preparation of controlled release fertilizer. Chem. Ind. Chem. Eng. Q. 20, 207–213. https://doi.org/10.2298/CICEQ121004001M.
Makó, É., Kristóf, J., Horváth, E., Vágvölgyi, V., 2009. Kaolinite–urea complexes obtained by mechanochemical and aqueous suspension techniques—a comparative study. J. Colloid Interface Sci. 330, 367–373. https://doi.org/10.1016/j.jcis.2008.10.054.
Makó, É., Kovács, A., Kristóf, T., 2019. Influencing parameters of direct homogenization intercalation of kaolinite with urea, dimethyl sulfoxide, formamide, and N-methylformamide. Appl. Clay Sci. 182, 105287. https://doi.org/10.1016/j.clay.2019.105287.
Marchesi, S., Bisio, C., Lalli, D., Marchese, L., Platas-Iglesias, C., Carniato, F., 2021. Bifunctional Paramagnetic and Luminescent Clays Obtained by Incorporation of Gd 3+ and Eu 3+ Ions in the Saponite Framework. Inorg. Chem. 60, 10749–10756. https://doi.org/10.1021/acs.inorgchem.1c01455.
Marsh, A., Heath, A., Patureau, P., Evernden, M., Walker, P., 2018. Alkali activation behaviour of un-calcined montmorillonite and illite clay minerals. Appl. Clay Sci. 166, 250–261. https://doi.org/10.1016/j.clay.2018.09.011.
Maruoka, L.M.A., Pinheiro, I.F., Freitas, H.S., Nobre, F.X., Scalvi, L.V.A., 2023. Effect of thermal annealing on kaolin from the Amazon region, aiming at the production of geopolymer. J. Mater. Res. Technol. 25, 2471–2485. https://doi.org/10.1016/j.jmrt.2023.06.105.
Mbey, J.A., Thomas, F., Ngally Sabouang, C.J., Liboum Njopwouo, D., 2013. An insight on the weakening of the interlayer bonds in a Cameroonian kaolinite through DMSO intercalation. Appl. Clay Sci. 83–84, 327–335. https://doi.org/10.1016/j.clay.2013.08.010.
Mbey, J.-A., Siéwé, J.M., Ngally Sabouang, C.J., Razafitianamaharavo, A., Kong, S., Thomas, F., 2020. DMSO intercalation in selected Kaolinites: influence of the crystallinity. ChemEngineering 4, 66. https://doi.org/10.3390/chemengineering4040066.
Mitchell, J.K., Soga, K., 2005. Fundamentals of Soil Behavior, 3rd ed. John Wiley & Sons, Inc, Hoboken, NJ, USA.
Mohammed, I., Al Shehri, D., Mahmoud, M., Kamal, M.S., Alade, O.S., 2021. A surface charge approach to investigating the influence of oil contacting clay minerals on wettability alteration. ACS Omega 6, 12841–12852. https://doi.org/10.1021/acsomega.1c01221.
Murray, H.H., 2006. Kaolin applications. In: Murray, H.H. (Ed.), Developments in Clay Science. Elsevier B.V, Bloomington, U.S.A, pp. 85–109. https://doi.org/10.1016/S1572-4352(06)02005-8.
Őze, C., Makó, É., 2023. Optimization of grinding parameters for the mechanochemical activation of Kaolin with the addition of trass. Minerals 13, 20. https://doi.org/10.3390/min13070915.
Păcurariu, C., Lazău, I., Lazău, R., 2017. Kinetic studies of the dehydroxylation and crystallization of raw kaolinite and fluorides-modified kaolinite. J. Therm. Anal. Calorim. 127, 239–246. https://doi.org/10.1007/s10973-016-5763-5.
Paiva, P.R.P., Monte, M.B.M., Falcão, G.F., 2005. Modificação química do caulim pelo método de intercalação. In: XXI Encontro Nacional de Tratamento de Minérios e Metalurgia Extrativa. ENTMME, Natal-RN, pp. 474–481.
Pazos, M.C., Bravo, L.R., Ramos, S.E., Osuna, F.J., Pavón, E., Alba, M.D., 2020. Multiple pollutants removal by functionalized heterostructures based on Na-2-Mica. Appl. Clay Sci. 196, 105749. https://doi.org/10.1016/j.clay.2020.105749.
Pei, P., Sun, T., Xu, Y., Sun, Y., 2022. Using thiol-functionalized montmorillonites for chemically immobilizing Hg in contaminated water and soil: a comparative study of intercalation and grafting functionalization. Appl. Clay Sci. 216, 106381. https://doi.org/10.1016/j.clay.2021.106381.
Ptáček, P., Kubátová, D., Havlica, J., Brandštetr, J., Šoukal, F., Opravil, T., 2010. The non-isothermal kinetic analysis of the thermal decomposition of kaolinite by thermogravimetric analysis. Powder Technol. 204, 222–227. https://doi.org/10.1016/j.powtec.2010.08.004.
Riello, P., 2004. Quantitative analysis of amorphous fraction in the study of the microstructure of semi-crystalline materials. In: Mittemeijer, E.J., Scardi, P. (Eds.), Diffraction Analysis of the Microstructure of Materials. Springer, Berlin Heidelberg, Berlin, Heidelberg, pp. 167–184. https://doi.org/10.1007/978-3-662-06723-9_7.
Rietveld, H.M., 1969. A profile refinement method for nuclear and magnetic structures. J. Appl. Crystallogr. 2, 65–71. https://doi.org/10.1107/S0021889869006558.

Saad, H., Turki, T., Srasra, M., Srasra, E., 2025. Sorption behavior of pomegranate polyphenols on surfactant-modified clays in aqueous solution. Sci. Afr. 27, e02568. https://doi.org/10.1016/j.sciaf.2025.e02568.

Sahnoune, F., Saheb, N., Khamel, B., Takkouk, Z., 2012. Thermal analysis of dehydroxylation of Algerian kaolinite. J. Therm. Anal. Calorim. 107, 1067–1072. https://doi.org/10.1007/s10973-011-1622-6.

Saikia, P., 2020. Clay nanostructures for biomedical applications. In: Khan, R., Barua, S. (Eds.), Two-Dimensional Nanostructures for Biomedical Technology. Elsevier, Amsterdam, Netherlands, pp. 137–172. https://doi.org/10.1016/B978-0-12-817650-4.00005-X.

Saikia, B.J., Parthasarathy, G., 2010. Fourier transform infrared spectroscopic characterization of kaolinite from Assam and Meghalaya, Northeastern India. J. Mod. Phys. 01, 206–210. https://doi.org/10.4236/jmp.2010.14031.

Sánchez-Soto, P.J., Jiménez, Carmen, de Haro, M., Pérez-Maqueda, L.A., Varona, I., Pérez-Rodríguez, J.L., 2004. Effects of dry grinding on the structural changes of kaolinite powders. J. Am. Ceram. Soc. 83, 1649–1657. https://doi.org/10.1111/j.1151-2916.2000.tb01444.x.

Sanusi, O.M., Benelfellah, A., Aït Hocine, N., 2020. Clays and carbon nanotubes as hybrid nanofillers in thermoplastic-based nanocomposites – a review. Appl. Clay Sci. 185, 105408. https://doi.org/10.1016/j.clay.2019.105408.

Sarkar, P., Ghimire, S., Vlasov, S., Mukhopadhyay, K., 2023. Effect of clay-zwitterionic interactions in controlling the viscoelastic properties in organomodified clays. iScience 26, 108388. https://doi.org/10.1016/j.isci.2023.108388.

Seifi, S., Diatta-Dieme, M.T., Blanchart, P., Lecomte-Nana, G.L., Kobor, D., Petit, S., 2016. Kaolin intercalated by urea. Ceramic applications. Constr. Build. Mater. 113, 579–585. https://doi.org/10.1016/j.conbuildmat.2016.03.095.

Soleimanpour Moghadam, N., Azadmehr, A., Hezarkhani, A., 2022. Extended release of 6-aminopenicillanic acid by silanol group functionalized vermiculite. J. Dispers. Sci. Technol. 43, 1231–1244. https://doi.org/10.1080/01932691.2020.1850291.

Stokes, G.G., 1844. On the Effect of the Internal Friction of Fluids on the Motion of Pendulums. Cambridge University Press, Cambridge, UK.

Stone, R.L., 1952. Differential thermal analysis of Kaolin group minerals under controlled partial pressures of H 2 O. J. Am. Ceram. Soc. 35, 90–99. https://doi.org/10.1111/j.1151-2916.1952.tb13077.x.

Tassongwa, B., Eba, F., Njoya, D., Tchakounté, J.N., Jeudong, N., Nkoumbou, C., Njopwouo, D., 2017. Physico-chemistry and geochemistry of Balengou clay deposit (West Cameroon) with inference to an argillic hydrothermal alteration. Compt. Rendus Geosci. 349, 212–222. https://doi.org/10.1016/j.crte.2017.06.002.

Tironi, A., Trezza, M.A., Irassar, E.F., Scian, A.N., 2012. Thermal treatment of Kaolin: effect on the Pozzolanic activity. Procedia Mater. Sci. 1, 343–350. https://doi.org/10.1016/j.mspro.2012.06.046.

Uehara, G., Gillman, G., 1981. The Mineralogy, Chemistry, and Physics of Tropical Soils with Variable Charge Clays. Westview Press Inc, Boulder, Colorado, U.S.A.

Valášková, M., Rieder, M., Matějka, V., Čapková, P., Slíva, A., 2007. Exfoliation/delamination of kaolinite by low-temperature washing of kaolinite–urea intercalates. Appl. Clay Sci. 35, 108–118. https://doi.org/10.1016/j.clay.2006.07.001.

Wiewiora, A., Brindley, G.W., 1969. Potassium acetate intercalation in kaolinite and its removal; effect of material characteristics. In: Proceedings of the International Clay Conference. Tokyo, Japan, pp. 723–733.

Worral, W.E., 1975. Clays and Ceramic Raw Materials, 1st ed. John Wiley & Sons Inc, London, UK.

Yilmaz, Y.Y., Yalcinkaya, E.E., Demirkol, D.O., Timur, S., 2020. 4-aminothiophenol-intercalated montmorillonite: organic-inorganic hybrid material as an immobilization support for biosensors. Sensors Actuators B Chem. 307, 127665. https://doi.org/10.1016/j.snb.2020.127665.

Yong, R.N., Mohamed, A.M.O., Warkentin, B.P., 1992. Principles of Contaminant Transport in Soils. Elsevier Science Publishers, Amsterdam, Netherlands.

Zaccaron, A., Benedet, G.A., Saviatto, E., Raupp-Pereira, F., Peterson, M., Ribeiro, M.J., Bernardin, A.M., 2025. Organic intercalation with dimethyl sulfoxide and diaminomethanal in the Kaolin organophilization process. J. Inorg. Organomet. Polym. Mater. In Press. https://doi.org/10.1007/s10904-025-03675-x.

Zaharia, A., Perrin, F.-X., Teodorescu, M., Radu, A.-L., Iordache, T.-V., Florea, A.-M., Donescu, D., Sarbu, A., 2015. New organophilic kaolin clays based on single-point grafted 3-aminopropyl dimethylethoxysilane. Phys. Chem. Chem. Phys. 17, 24908–24916. https://doi.org/10.1039/C5CP04395F.

Zare, Y., Rhee, K.Y., 2020. Simulation of Young's modulus for clay-reinforced nanocomposites assuming mechanical percolation, clay-interphase networks and interfacial linkage. J. Mater. Res. Technol. 9, 12473–12483. https://doi.org/10.1016/j.jmrt.2020.08.097.

Zhang, S., Liu, Q., Cheng, H., Li, X., Zeng, F., Frost, R.L., 2014. Intercalation of dodecylamine into kaolinite and its layering structure investigated by molecular dynamics simulation. J. Colloid Interface Sci. 430, 345–350. https://doi.org/10.1016/j.jcis.2014.05.059.

Zhang, S., Liu, Q., Cheng, H., Zeng, F., 2015. Combined experimental and theoretical investigation of interactions between kaolinite inner surface and intercalated dimethyl sulfoxide. Appl. Surf. Sci. 331, 234–240. https://doi.org/10.1016/j.apsusc.2015.01.019.

Zhang, S., Liu, Q., Gao, F., Li, X., Liu, C., Li, H., Boyd, S.A., Johnston, C.T., Teppen, B.J., 2017. Mechanism associated with kaolinite intercalation with urea: combination of infrared spectroscopy and molecular dynamics simulation studies. J. Phys. Chem. C 121, 402–409. https://doi.org/10.1021/acs.jpcc.6b10533.

Zhu, X., Yan, C., Chen, J., 2012. Application of urea-intercalated kaolinite for paper coating. Appl. Clay Sci. 55, 114–119. https://doi.org/10.1016/j.clay.2011.11.001.